inorganics

MDPI

Article

Phase Formation of Co and Cr Co-Doped Bismuth Niobate with Pyrochlore Structure

Nadezhda A. Zhuk [1,*], Ksenia A. Badanina [1], Roman I. Korolev [1], Boris A. Makeev [2], Maria G. Krzhizhanovskaya [3] and Vladislav V. Kharton [4]

[1] Institute of Natural Sciences, Syktyvkar State University, Oktyabrsky Prospect, 55, 167001 Syktyvkar, Russia; badanina-ksenia@mail.ru (K.A.B.); korolev36a@gmail.com (R.I.K.)
[2] Institute of Geology of the Komi Science Center UB RAS, Pervomaiskaya st. 48, 167982 Syktyvkar, Russia; makboris@mail.ru
[3] Institute of Earth Sciences, Saint Petersburg State University, University Emb. 7/9, 199034 St. Petersburg, Russia; krzhizhanovskaya@mail.ru
[4] Osipyan Institute of Solid State Physics RAS, 142432 Chernogolovka, Russia; kharton@issp.ac.ru
* Correspondence: nzhuck@mail.ru

Abstract: The formation mechanisms of pyrochlore-type $Bi_2Co_{1/2}Cr_{1/2}Nb_2O_{9+\Delta}$ (space group Fd-3m, a = 10.4838(8) Å), in the temperature range from 400 to 1050 °C were studied by employing X-ray diffraction, scanning electron microscopy and energy-dispersive spectroscopy. An extensive reaction between the binary metal oxides was found to begin at temperatures above 550 °C, following the transition of monoclinic α-Bi_2O_3 into a tetragonal β-Bi_2O_3 polymorph. The synthesis process occurs in several stages when Bi-rich intermediate products (Bi_6CrO_{12}, $Bi_6Cr_2O_{15}$, and $Bi_5Nb_3O_{15}$) transform into bismuth-depleted $BiNbO_4$ and a chromium–cobalt spinel is formed. The formation of a single pyrochlore phase occurs at the final reaction stage at 1050 °C via the doping of bismuth ortho-niobate, $BiNbO_4$, by the transition metal cations. The observed mechanism is essentially similar to the mechanism of tantalate-based phases except for the formation of $Bi_5Nb_3O_{15}$ at the intermediate reaction stages.

Keywords: pyrochlore; pyrochlore; phase formation; Co and Cr co-doping

check for updates

Citation: Zhuk, N.A.; Badanina, K.A.; Korolev, R.I.; Makeev, B.A.; Krzhizhanovskaya, M.G.; Kharton, V.V. Phase Formation of Co and Cr Co-Doped Bismuth Niobate with Pyrochlore Structure. *Inorganics* **2023**, *11*, 288. https://doi.org/10.3390/inorganics11070288

Academic Editors: Axel Klein and Michael A. Hayward

Received: 25 May 2023
Revised: 29 June 2023
Accepted: 29 June 2023
Published: 3 July 2023

1. Introduction

Bismuth-containing oxide phases with $A_2B_2O_6O'$ pyrochlore structures possess unique dielectric and photocatalytic properties, promising a variety of potential applications [1–4]. This crystal structure may be considered to consist of two in the course of the solid-state synthesis of Bi A_2O and B_2O_6 units [5,6]. The framework of B_2O_6 octahedra with relatively small A cations comprises voids accommodating large A cations, such as Bi^{3+}, and one additional O′ anion per each $(BO_3)_2$ formula unit. The tolerance of this structure with respect to cation substitutions and vacancy formation in the oxygen sites and in one of cationic sublattices makes it possible to vary the compositions and functional properties of the pyrochlore-based materials. In recent decades, a significant amount of attention has been focused on bismuth tantalate and niobate pyrochlores [7–16]. The important features of these phases refer to cation vacancies in the bismuth sublattice and the distribution of 3D transition metal cations between both A and B sites, leading to attractive relaxation phenomena [17,18]. For instance, ceramic materials made of bismuth tantalate doped with transition metal cations (Cu, Ni, Fe, Cr, Co, and Zn) exhibit the low dielectric losses and moderate dielectric permittivity values necessary for practical applications [3,8,12,19–21]. High values of permittivity, 141–151, and dielectric loss, ~0.2, at 30 °C and 1 MHz are exhibited by pyrochlores in the Bi_2O_3-Fe_2O_3-Nb_2O_5 system [22]. The dielectric characteristics of pyrochlores based on bismuth tantalate are much more modest, which is explained by the formation of highly porous ceramics. It is shown that

iron-containing pyrochlores, $Bi_{3.36}Fe_{2.08+x}Ta_{2.56-x}O_{14.56-x}$ ($-0.32 \leq x \leq 0.48$), exhibit lower dielectric constant (∼78–92) and dielectric loss tangent (~10^{-1}) (MHz, ~30 °C) values [23]. $Bi_{2.48+y}Cu_{1.92-x}Ta_{3.6+x-y}O_{14.6+3x/2-y}$ solid solutions [24] demonstrate moderate values of permittivity ($\varepsilon \approx$ 60–80) and dielectric loss (tanδ = 0.01–0.20, RT, 1MHz). Magnesium-containing pyrochlores, $Bi_{3+5/2x}Mg_{2-x}Ta_{3-3/2x}O_{14-x}$ ($0.12 \leq x \leq 0.22$), are characterized by comparable values of ε~70–85 and a low dielectric loss tangent δ~10^{-3} at 1 MHz and 30 °C [25,26]. For the pyrochlore $Bi_{1.5}ZnTa_{1.5}O_7$, the permittivity is 58 [27,28]. The electrical characteristics of cobalt pyrochlores are comparable to those of nickel- and magnesium-containing preparations of the similar composition $Bi_2Mg(Ni)Ta_2O_9$, the permittivity and dielectric loss tangent of which are 20 (32) and 2×10^{-3}(6×10^{-2}) at RT and a frequency of 1 MHz [29,30]. As shown in [31], $Bi_2Mg_{1-x}Ni_xTa_2O_9$ (x = 0.3, 0.5, 0.7) samples are insulators, with high activation energies of ~2.0 eV, average values of permittivity (~24–28) and a dielectric loss of ~0.002 at 1 MHz and 21 °C.

Investigations of the pyrochlore phase formation mechanisms in these materials revealed key stages of the solid-state reactions, including the appearance of α-$BiTaO_4$ as an intermediate product transforming into pyrochlore [32–36]. In the case of chromium doping, intermediate phases containing Cr(VI) were found to form [35]. Continuing this research, the present work focused on the analysis of pyrochlore formation in bismuth niobate co-doped with chromium and cobalt, and its comparison with tantalate-based oxide systems. The purpose of the experiment was to determine the optimal conditions for the synthesis of multielement pyrochlore based on bismuth niobate and to identify differences with pyrochlores based on bismuth tantalate.

2. Experimental

The solid-state synthesis of $Bi_2Co_{1/2}Cr_{1/2}Nb_2O_{9+\Delta}$ samples was carried out using high-purity Bi_2O_3, Nb_2O_5, Cr_2O_3 and Co_3O_4 (all analytical reagent grade) as starting materials. The oxides were taken in such molar ratios n(Bi_2O_3):n(Nb_2O_5):n(Cr_2O_3):n(Co_3O_4) = 1:1:1/4:1/6. The mass of bismuth oxide was 2 g. The stoichiometric mixtures were carefully homogenized using an agate mortar for one hour and then pressed into disks. For the studies of phase formation process, the samples were sequentially calcined in air at temperatures from 400 to 1050 °C (in steps of 50 °C) for 10 and 15 h at each stage of the solid-state reaction. After each calcining step, the samples were ground, homogenized and pressed into disks again. X-ray diffraction (XRD) patterns were collected by employing a Shimadzu 6000 instrument (CuK_α-radiation; 2θ = 10–80°; scanning rate of 2.0°/min). The microstructure and elemental distribution were studied via scanning electron microscopy coupled with energy-dispersive spectroscopy (SEM/EDS, Tescan VEGA 3LMN microscope equipped with an INCA Energy 450 spectrometer). The unit cell parameters were refined by the Topas 5.0 program, employing the Pawley approach and using CSD software (CSD-4,CSD-universal program package for single crystal and powder structure data treatment, Russia, Akselrud, L.G. et al) [37]. The background was described by 12 Chebyshev polynomials, and the peak shape was modelled via the Thompson–Cox–Hastings pseudo-Voigt function.

3. Results and Discussion

The pyrochlore phase evolution in the temperature range of 400–1050 °C was analyzed using the example of $Bi_2Co_{1/2}Cr_{1/2}Nb_2O_{9+\Delta}$, a model composition with equal concentrations of cobalt and chromium cations. This composition was selected due to the existence of single pyrochlore phases in Cr- and Co- co-doped bismuth tantalate systems reported elsewhere [21,38], and due to the positive effects of the chromium and cobalt additions observed in the course of the solid-state synthesis of $Bi_2Mg(Zn)_{1-x}M_xTa_2O_{9.5-\Delta}$ (M = Cr, Fe) and $Bi_2Cr_{1/6}Mn_{1/6}Fe_{1/6}Co_{1/6}Ni_{1/6}Cu_{1/6}Ta_2O_{9+\Delta}$ pyrochlores [34,35]. Figures 1 and 2 display XRD patterns of the $Bi_2Co_{1/2}Cr_{1/2}Nb_2O_{9+\Delta}$ after calcining at different temperatures. A summary of the phase composition, determined from the XRD and SEM results, is presented in Table 1.

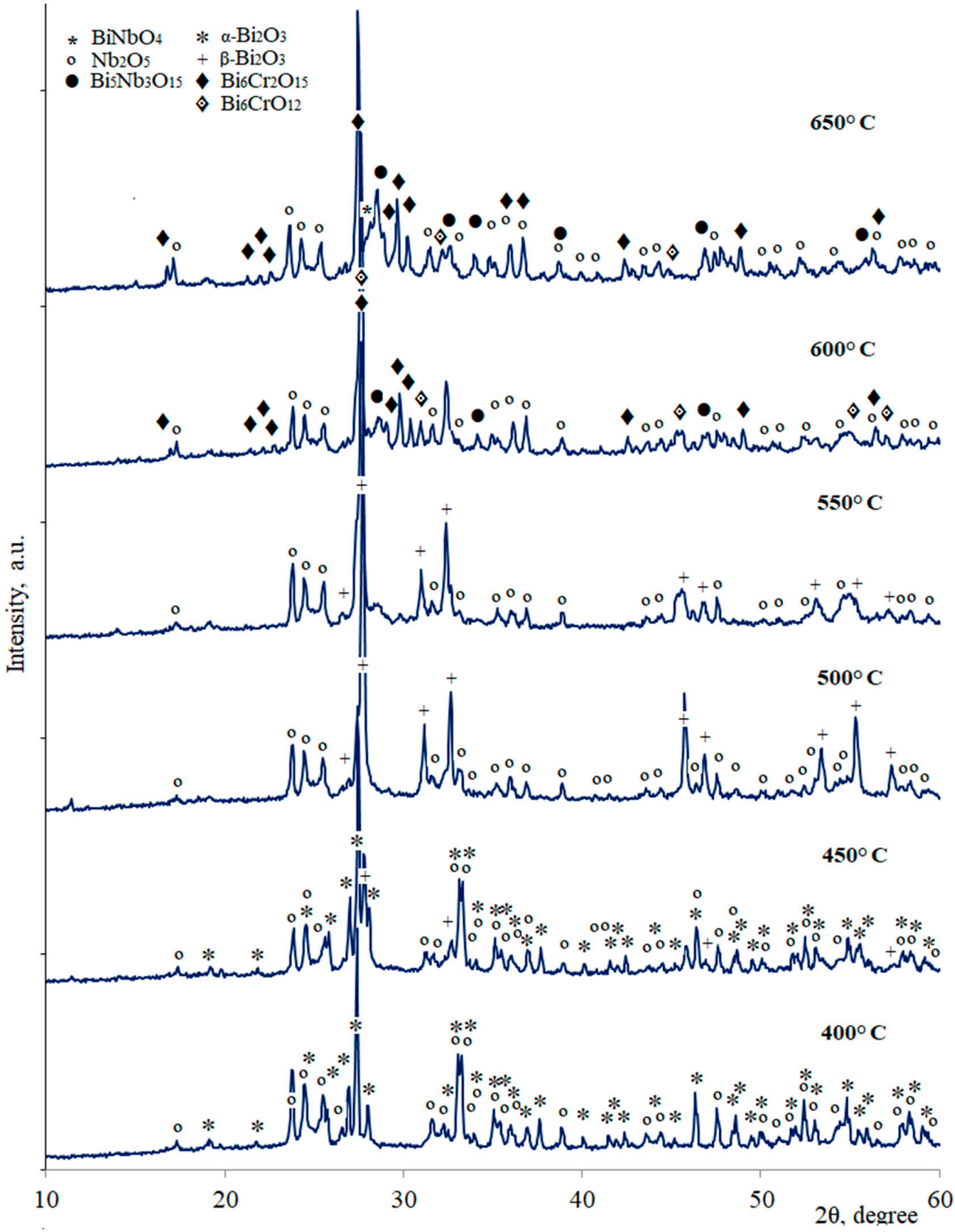

Figure 1. XRD patterns of $Bi_2Co_{1/2}Cr_{1/2}Nb_2O_{9+\Delta}$ calcined at temperatures from 400 to 650 °C (10 h each step).

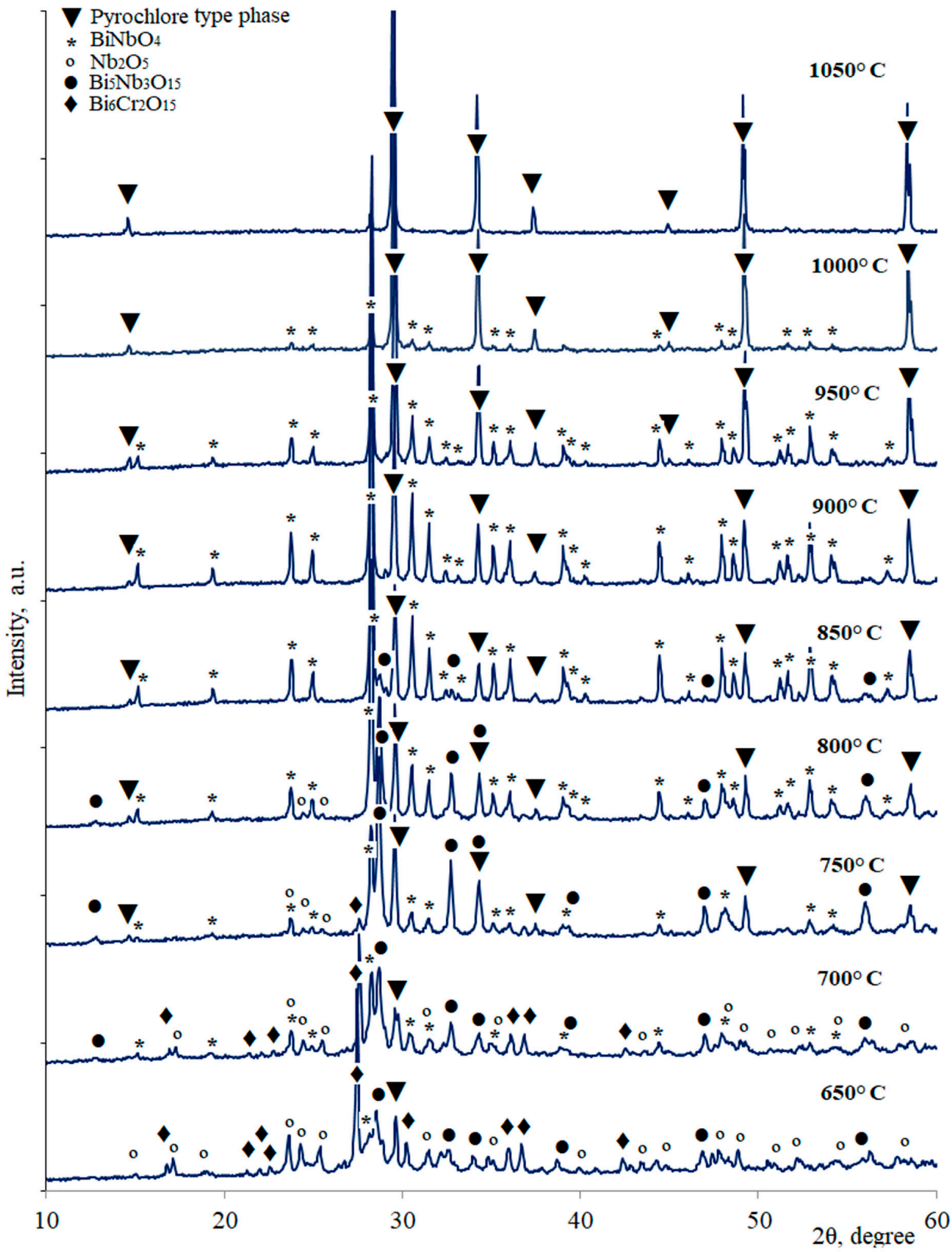

Figure 2. XRD patterns of $Bi_2Co_{1/2}Cr_{1/2}Nb_2O_{9+\Delta}$ calcined at temperatures from 650 to 1050 °C (10 h each step).

Table 1. Phase composition of $Bi_2Co_{1/2}Cr_{1/2}Nb_2O_{9+\Delta}$ as a function of calcining temperature, evaluated from the XRD and SEM/EDS results.

Annealing Temperature, °C	Phase Composition
400	Nb_2O_5, α-Bi_2O_3
450	Nb_2O_5, α-Bi_2O_3, β-Bi_2O_3
500–550	Nb_2O_5, β-Bi_2O_3
600	Nb_2O_5, $Bi_5Nb_3O_{15}$(traces), Bi_6CrO_{12}, $Bi_6Cr_2O_{15}$
650	Nb_2O_5, $Bi_5Nb_3O_{15}$, $Bi_6Cr_2O_{15}$, $BiNbO_4$(traces), pyrochlore (traces)
700	Nb_2O_5, $Bi_5Nb_3O_{15}$, $Bi_6Cr_2O_{15}$ (traces), $BiNbO_4$, pyrochlore
750	Nb_2O_5, $Bi_5Nb_3O_{15}$, $BiNbO_4$, pyrochlore
800	Nb_2O_5 (traces), $Bi_5Nb_3O_{15}$, $BiNbO_4$, pyrochlore
850	Pyrochlore, $Bi_5Nb_3O_{15}$(traces), $BiNbO_4$
900–1000	Pyrochlore, $BiNbO_4$
1050	Pyrochlore

In the low-temperature range, 400–450 °C, the XRD patterns comprise peaks of the starting binary metal oxides, in particular, β-Nb_2O_5 [39] and monoclinic α-Bi_2O_3 [40] (Figure 1). At temperatures around 500 °C, the latter phase with space group (S.G.) P21/c transforms into a tetragonal β-Bi_2O_3 polymorph (S.G. P-421c). At 600 °C, the products of the bismuth oxide reaction with chromium and niobium oxides, namely, $Bi_5Nb_3O_{15}$ (S.G. P4/mmm), Bi_6CrO_{12} and $Bi_6Cr_2O_{15}$ (S.G. Ccc2) [41–43], appear in the XRD patterns. The formation of chromium (VI) compounds is responsible for the orange-brown color of the ceramic samples annealed at 500–650 °C (Figure 3). Notice that the intermediate products containing Cr(VI) were detected earlier during the synthesis of $Bi_2Mg(Zn)_{1-x}Cr_xTa_2O_{9.5-\Delta}$ pyrochlores up to 700 °C [35].

When the calcining temperature increases up to 650 °C, the bismuth-rich Bi_6CrO_{12} transforms into $Bi_6Cr_2O_{15}$, which may be associated with parallel reactions resulting in the formation of $Bi_5Nb_3O_{15}$ and orthorhombic α-$BiNbO_4$ (S.G. Pnna). Such behavior originates from the higher level of chemical reactivity of bismuth oxide compared to niobia. An extensive interaction of the components begins to occur at temperatures of 650 °C and above. At 650 °C, XRD patterns exhibit the reflections of monoclinic β-Nb_2O_5 (пр.гр. P2/m), $Bi_6Cr_2O_{15}$, $Bi_5Nb_3O_1$, and pyrochlore and $BiNbO_4$ in trace amounts (Table 1). No peaks of niobia are observed for the samples calcined at temperatures of 850 °C and higher; $Bi_6Cr_2O_{15}$ and $Bi_5Nb_3O_{15}$ disappear at 750 °C and 900 °C, respectively. The thermal dissociation of $Bi_6Cr_2O_{15}$ into Cr(III)-containing compounds causes the green color of the materials annealed above 700 °C (Figure 3). Significant amounts of the pyrochlore phase begin to appear at 750 °C, when the contents of Nb_2O_5 and $Bi_6Cr_2O_{15}$ substantially decrease. This indicates that the pyrochlore formation kinetics are essentially governed by the chemical inertness of Nb_2O_5. One should also mention that the intermediate product in the pyrochlore synthesis reaction is $Bi_5Nb_3O_{15}$; its Bi-rich analogue in the synthesis of pyrochlore-type bismuth tantalate was, however, Bi_3TaO_7 (S.G. Fm-3m) [44], and isostructural Bi_3NbO_7 is also known in the literature [45]. Upon a further increase in the calcination temperature, $Bi_5Nb_3O_{15}$ turns into α-$BiNbO_4$ [46,47]; the dissolution of chromium and cobalt cations in the latter phase results in the final pyrochlore formation. In the temperature range of 900–1000 °C, XRD patterns demonstrate the co-existence of the pyrochlore and α-$BiNbO_4$ (Figure 2).

No reflections of chromium and cobalt oxides can be distinguished in the XRD patterns due to relatively small amounts of these components in the reacting mixtures and peak overlapping. In order to assess the transition metal cation distribution, EDS mapping of the ceramic samples annealed at 650–1050 °C was performed (Figures 4 and S1).

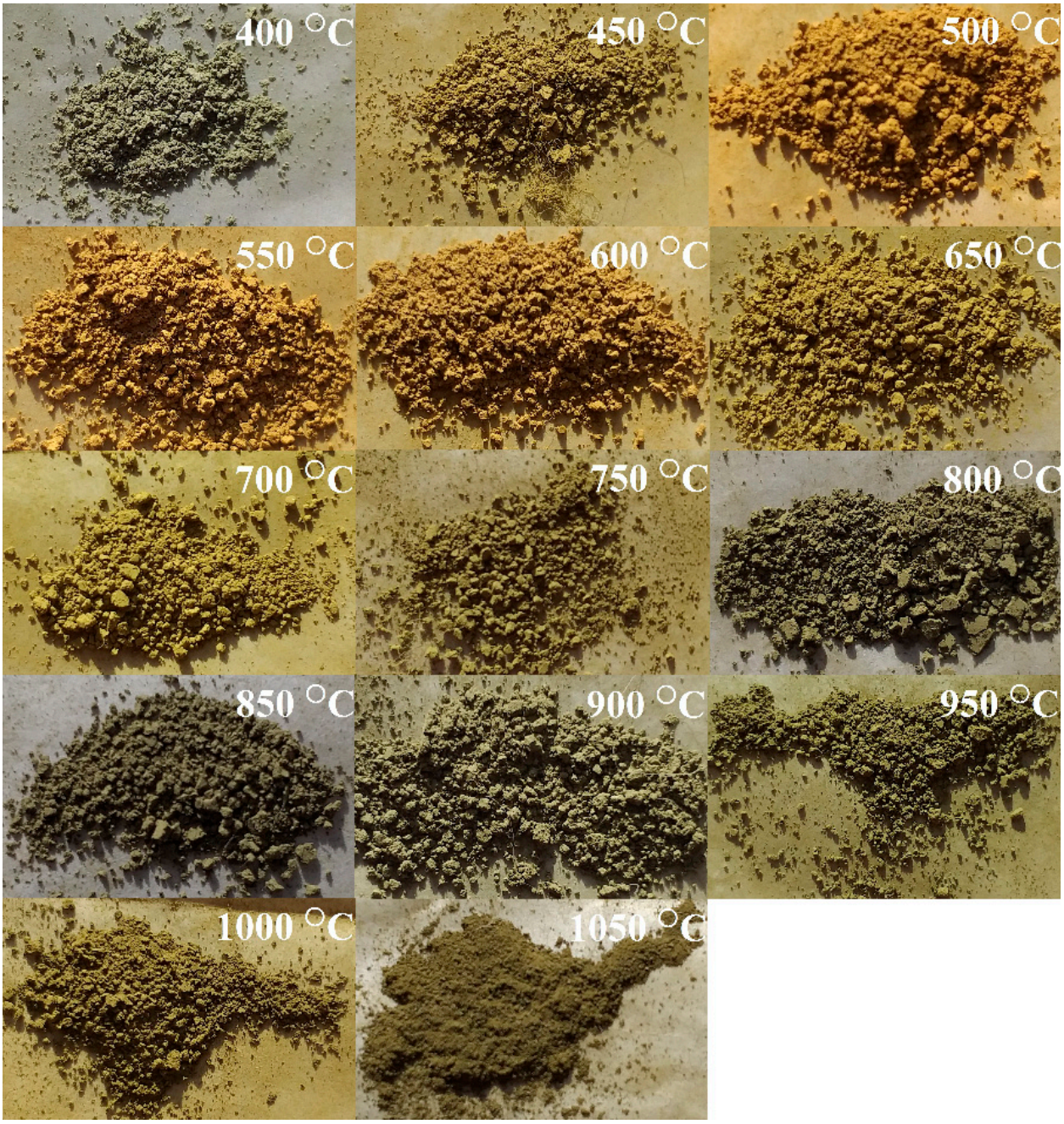

Figure 3. Colors of the powdered $Bi_2Co_{1/2}Cr_{1/2}Nb_2O_{9+\Delta}$ samples after calcining in the temperature range of 650–1050 °C.

The results show, in particular, that Cr and Co cations tend to concentrate in the same zones (Figure 5). This trend may indicate the formation of ternary chromium–cobalt oxide compounds at the intermediate reaction stages.

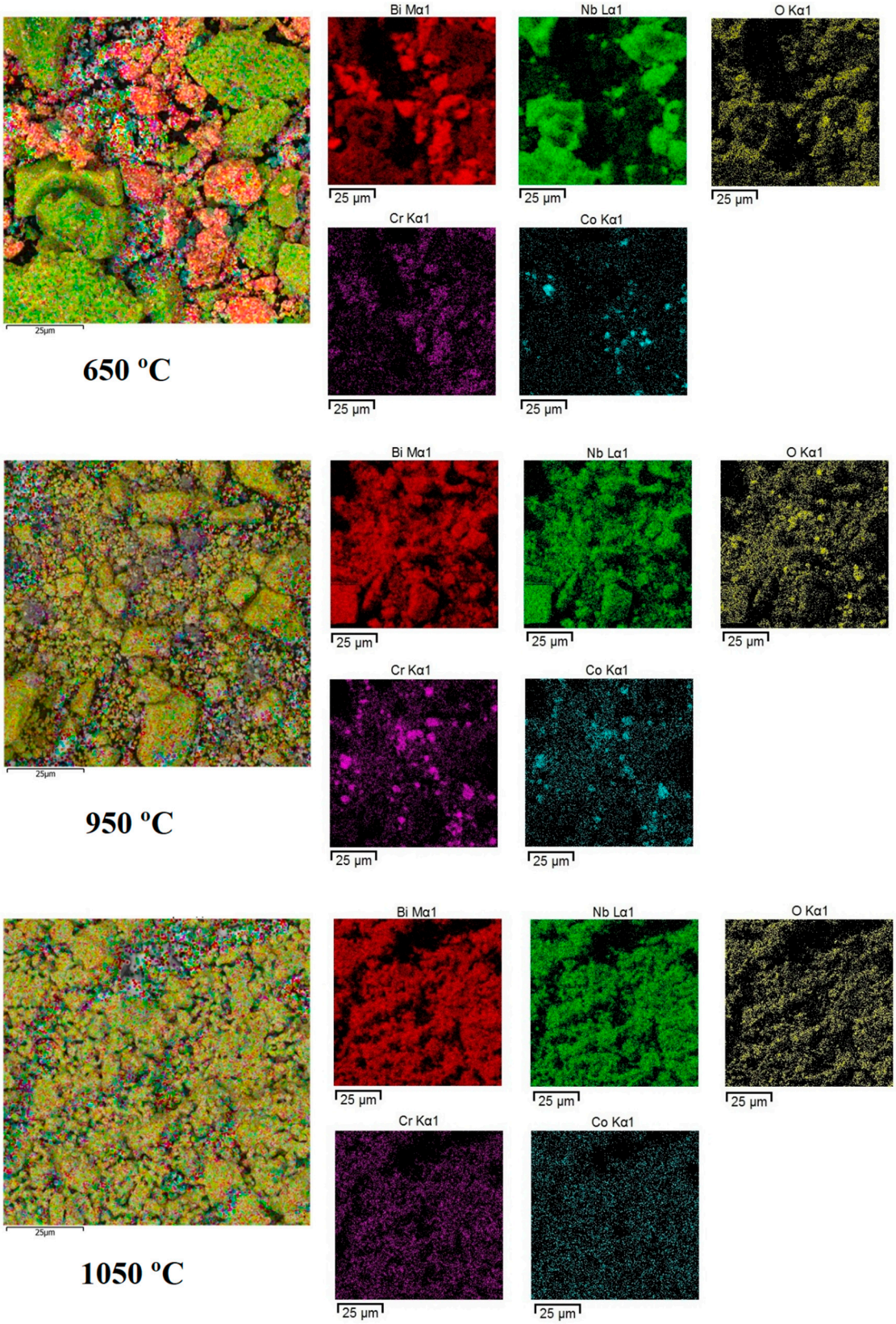

Figure 4. EDX elemental mapping of the $Bi_2Co_{1/2}Cr_{1/2}Nb_2O_{9+\Delta}$ samples, synthesized at the temperatures 650, 950 and 1050 °C.

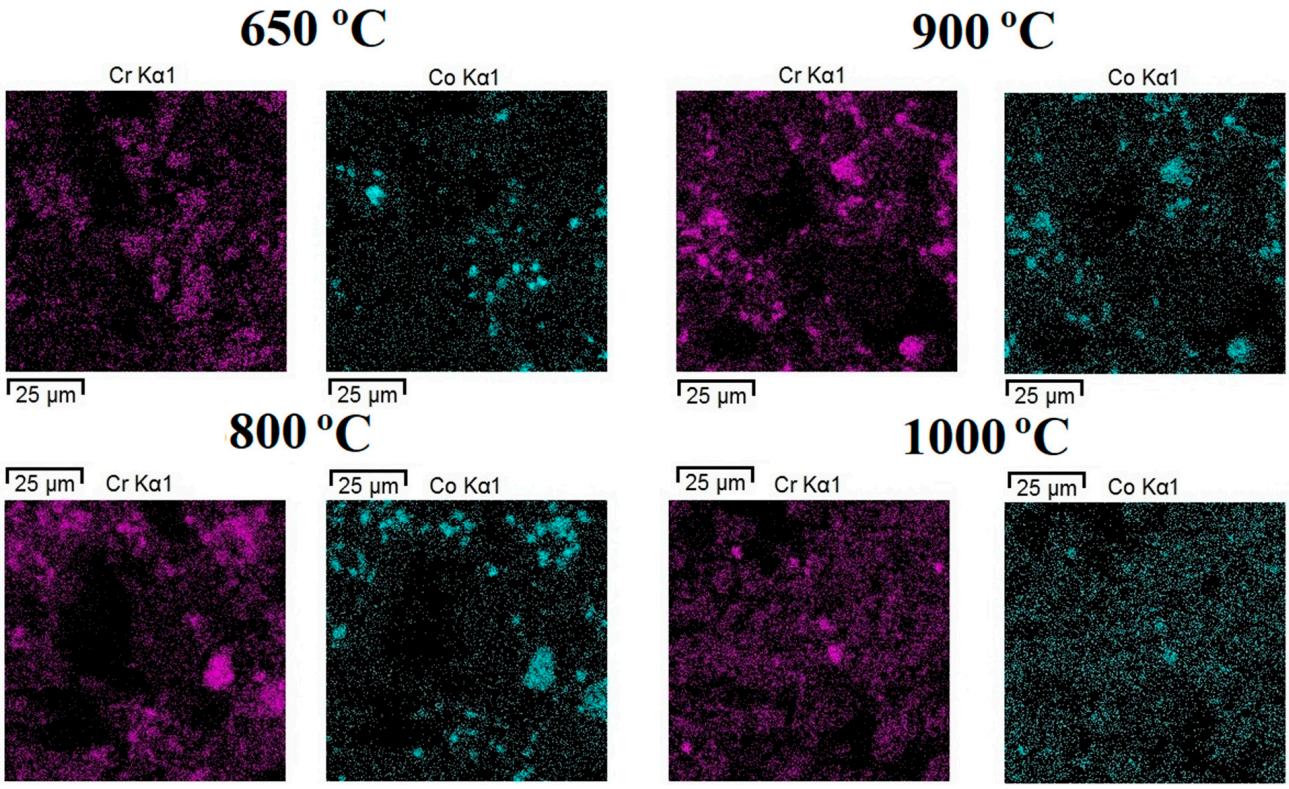

Figure 5. Distribution maps of Co and Cr cations in $Bi_2Co_{1/2}Cr_{1/2}Nb_2O_{9+\Delta}$, ceramics annealed at 650, 800, 900 and 1050 °C.

Indeed, the EDS analysis demonstrated that the compositions of the Co- and Cr-enriched zones are close to the spinel $CrCo_2O_4$ (i.e., $Co^{+2}Cr^{+3}Co^{+3}O_4$) [48]. In accordance with the XRD and EDS results, a single pyrochlore phase with uniform distribution of all the components was only obtained at the final calcination temperature, 1050 °C. Note that increasing the calcination time from 10 to 15 h at each annealing stage did not lead to any qualitative changes in the phase composition; only the concentration ratio between the main reaction products was altered (Table S1, Figure S2). One should mention that the content of the $BiNbO_4$ phase becomes larger as the thermal treatment time increases. This behavior originates from the grain growth at relatively low temperatures, hampering further reaction between the phases.

On the basis of these results, the following approximate mechanism of the pyrochlore phase formation can be suggested:

550–600 °C

$$5Bi_2O_3 + 3Nb_2O_5 = 2Bi_5Nb_3O_{15};$$

$$6Bi_2O_3 + Cr_2O_3 + 3/2O_2 = 2Bi_6CrO_{12}$$

$$6Bi_2O_3 + 2Cr_2O_3 + 3O_2 = 2Bi_6Cr_2O_{15}$$

650–750 °C

$$Bi_5Nb_3O_{15} + Nb_2O_5 = 5BiNbO_4$$

$$2Bi_6CrO_{12} + 1.8Nb_2O_5 = Bi_6Cr_2O_{15+}1.2Bi_5Nb_3O_{15}$$

$$Bi_6Cr_2O_{15} + 2.2Nb_2O_5 + Co_3O_4 = Bi_2Cr_{0.5}Nb_2O_{9+\Delta} + 0.8Bi_5Nb_3O_{15} + 1.5CrCo_2O_4 + (1.5\text{-}0.5\Delta)O_2$$

750–1050 °C

$$Bi_5Nb_3O_{15} + Nb_2O_5 = 5BiNbO_4$$

$$2BiNbO_4 + 0.5CrCo_2O_4 + Bi_2Cr_{0.5}Nb_2O_{9+\Delta} = 2Bi_2Cr_{0.5}Co_{0.5}Nb_2O_{9+\Delta}$$

In these equations, a tentative $Bi_2Cr_{0.5}Nb_2O_{9+\Delta}$ pyrochlore formula is used in order to emphasize the higher reactivity of the Cr(III) compounds with respect to cobalt and the only possibility of pyrochlore formation via the $BiNbO_4$ reaction.

The formation of bismuth-rich compounds in the early stages of the synthesis could be due to the high reactivity of bismuth oxide and the low reactivity of niobium(V) oxide. The second reason is the inhomogeneity of the mixture of precursors, which causes local concentrations of certain precursor phases in ceramics. The third reason may be that the interaction of bismuth oxide with the reagents proceeds through their dissolution in the oxide and the formation of solid solutions with large excesses of the fraction of bismuth atoms. With an increase in the calcination temperatures of the samples, the reactivity of niobium(V) oxide increases, which causes its interaction with the bismuth compounds to form bismuth-poor compounds.

Figure 6 displays typical SEM micrographs of multi- and single-phase $Bi_2Cr_{0.5}Co_{0.5}Nb_2O_{9+\Delta}$ ceramics sintered in the temperature range of 650–1050 °C. At temperatures below 1050 °C, the microstructures are clearly inhomogeneous, with a variety of inclusions formed by the impurity phases. The final reaction stage at 1050 °C leads to the densification and homogenization of the material. The energy-dispersive spectroscopy (Figure S3) showed that its chemical composition, $Bi_{0.95}Co_{0.50}Cr_{0.51}Nb_2O_{9+\Delta}$, is nominal within the limits of the experimental uncertainty of the EDS technique. The full-profile Rietveld refinement of the corresponding XRD pattern (Figure 7) confirmed the formation of a single pyrochlore phase.

The cubic unit cell parameter of the $Bi_2Cr_{0.5}Co_{0.5}Nb_2O_{9+\Delta}$ pyrochlore (S.G. Fd-3m) is equal to 10.4838(8) Å (Figure S3). This value is higher than that of the chromium-containing $Bi_2CrNb_2O_{9+y}$ (a = 10.459(2) Å) [49], in agreement with larger radius of the Co(II) cations with respect to Cr(III): R(Cr(III) = 0.615 Å and $R(Co(II))_{c.n.-6}$ = 0.745 Å [50]. Taking into account that ionic radii of Ta(V) and Nb(V) are equal to one another ($(R(Nb(V)/Ta(V))_{c.n.-6}$ = 0,64 Å) [50], the unit call parameters of the pyrochlore phases based on bismuth niobate and tantalate should be comparable. Indeed, the parameter of $Bi_2CrTa_2O_{9+\Delta}$ (a = 10.45523(3) Å) [21] is similar to that of the Cr-containing bismuth niobate. At the same time, the parameter of the $Bi_2Cr_{0.5}Co_{0.5}Nb_2O_{9+\Delta}$ synthesized in this work is close to that of $Bi_2Cr_{0.5}Mg_{0.5}Nb_2O_{9+\Delta}$ (a = 10.47702 Å) [51], again due to the similarity of the ionic radii of magnesium and cobalt (R(Mg(II) = 0.72 Å and $R(Co(II))_{c.n.-6}$ = 0.745 Å) [50].

We followed the nature of the change in the unit cell parameter of the pyrochlore with an increase in the calcination temperature of the samples calcined for 10 and 15 h. (Figure 8). As can be seen from the figure, in the course of synthesis, the unit cell parameter generally increases for both series of samples, but at different rates. The samples calcined from 400 °C for 10 h are characterized by higher values of the cell constant compared to the samples calcined from 650 °C for 15 h each. The differences can be considered significant, since the calculation of the unit cell parameters of the newly prepared samples and samples calcined in the range of 650–1050 °C for 15 h showed similar results. First of all, it should be noted that the cell parameter increases almost uniformly over the entire temperature range for both series of samples. Apparently, this is due to the inclusion of large ions, for example, Co(II) ions, into the pyrochlore phase as a result of a high-temperature solid-phase reaction. As shown in [34], Co(II) and Ni(II) oxides interact at elevated temperatures. In addition, as shown above, an impurity phase of a complex cobalt–chromium oxide of the $CrCo_2O_4$ type was found in the samples synthesized up to 1000 °C. Significant differences in the cell constant are observed in the range of 750–950 °C, which may be due to the most productive synthesis of the pyrochlore phase in the samples

calcined for 10 h. This is indicated by the smaller amounts of $BiNbO_4$ impurity in the samples calcined for 10 h. This seeming contradiction is resolved if we take into account the repeated homogenization of the samples of this series. Indeed, after calcination at 400 °C, the samples were crushed and thoroughly mixed. Apparently, the repeated procedure of the fragmentation and homogenization of the samples, starting from low calcination temperatures (400 °C), affected the accelerated synthesis of the pyrochlore phase in these samples. In addition, the shorter duration of calcination did not contribute to the growth of the ceramic grains. This had a positive effect on the synthesis and phase compositions of the ceramics. The close values of the unit cell parameters of the pyrochlore phase in the samples of both series and between themselves at temperatures of 950 and 1000 °C, 10.4670 Å and 10.4702 Å and 10.4708 Å and 10.4681 Å, respectively, may indicate that the completion of the synthesis process is close. It is interesting to note that for tantalum pyrochlores, the change in the unit cell parameter was different. No monotonic growth of the cell constant was observed. Apparently, this difference is associated with the reactivity of niobium(V) oxide and mainly the high-temperature formation of the pyrochlore phase. The method of scanning electron microscopy did not show the presence of a bismuth orthoniobate impurity in the sample calcined at 1050 °C. A quantitative analysis of the sample via the EDS method showed (Figure S3) that the chemical composition of the sample practically corresponded to the specified composition $Bi_{0.95}Co_{0.50}Cr_{0.51}Nb_2O_{9+\Delta}$.

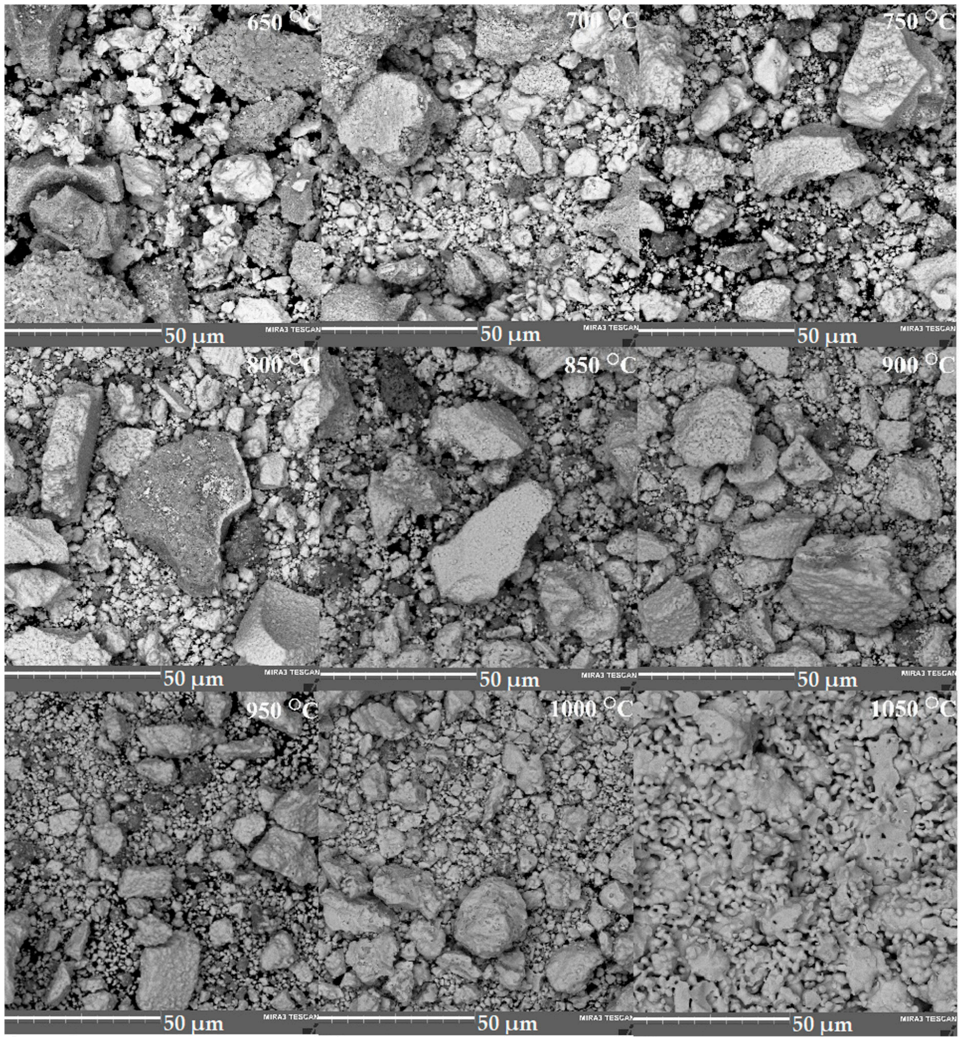

Figure 6. SEM images of the surface microstructures of $Bi_2Cr_{0.5}Co_{0.5}Nb_2O_{9+\Delta}$ ceramics annealed at temperatures from 650 to 1050 °C.

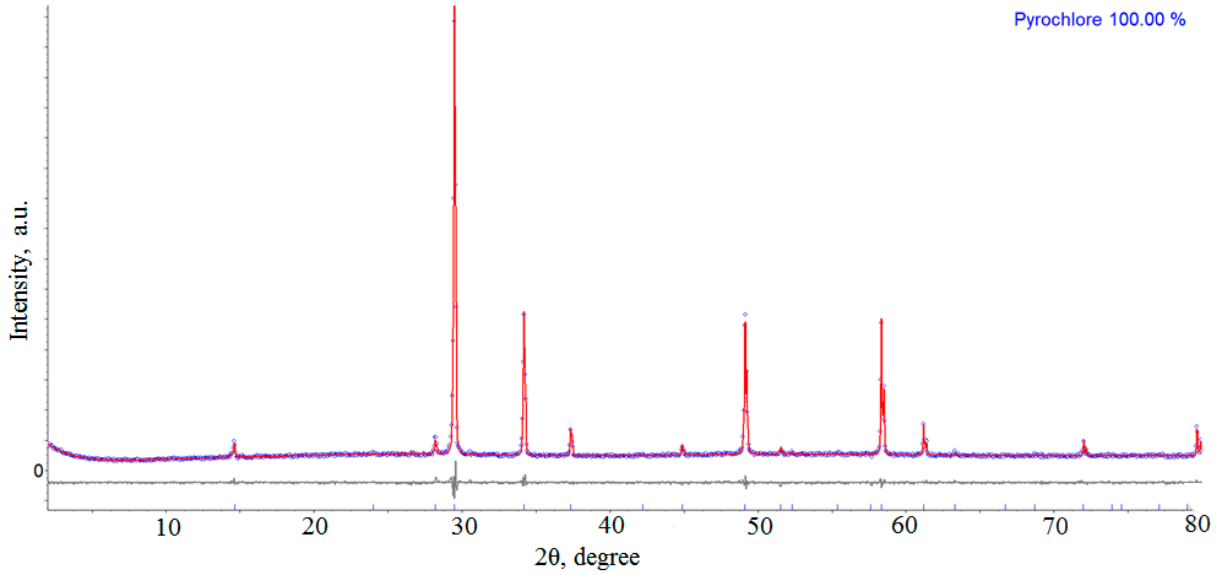

Figure 7. Rietveld refinement results for $Bi_2Cr_{0.5}Co_{0.5}Nb_2O_{9+\Delta}$ pyrochlore synthesized at 1050 °C.

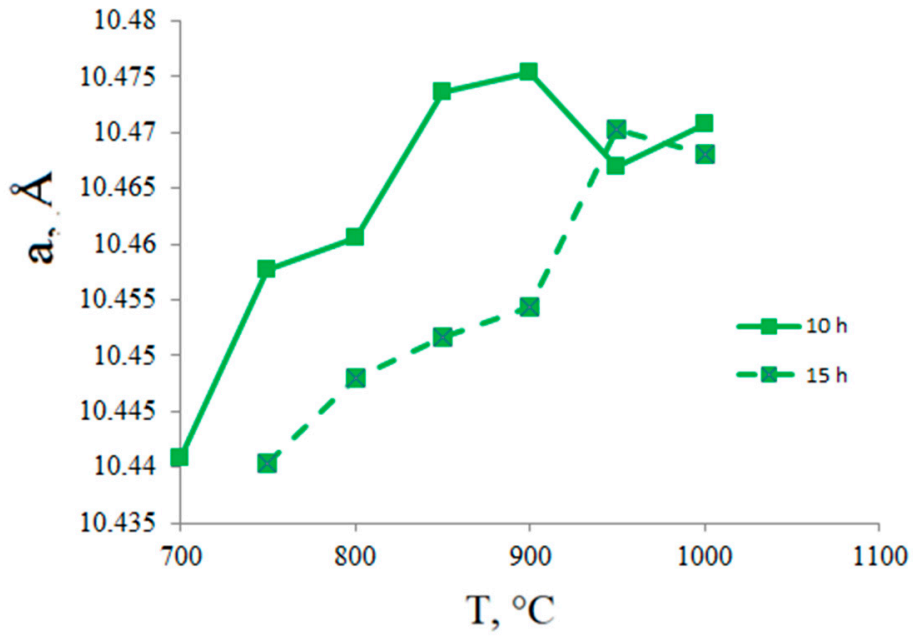

Figure 8. Changes in the unit cell parameter of the pyrochlore phase in the $Bi_2Cr_{0.5}Co_{0.5}Nb_2O_{9+\Delta}$ sample depending on the temperature and time of calcination at each stage.

4. Conclusions

The process of $Bi_2Co_{1/2}Cr_{1/2}Nb_2O_{9+\Delta}$ pyrochlore formation was studied in the temperature range of 400–1050 °C. An extensive reaction between the binary metal oxides begins at temperatures above 550 °C, following the transition of monoclinic α-Bi_2O_3 into a tetragonal β-Bi_2O_3 polymorph. The synthesis occurs in several stages when the Bi-rich oxide compounds transform into Bi-depleted ones and a chromium–cobalt spinel is formed. The pyrochlore formation occurs via the doping of bismuth orthoniobate by the transition metal cations. The final reaction stage resulting in single pyrochlore phase, accompanied with significant densification of the ceramics, was only observed at 1050 °C. The unit cell parameter of the pyrochlore phase increases over the entire temperature range studied. Cobalt and chromium oxides interact with each other, forming a complex oxide that is fixed as an independent phase up to 1000 °C.

Supplementary Materials: The following supporting information can be downloaded at: https://www.mdpi.com/article/10.3390/inorganics11070288/s1, Figure S1: EDS elemental mapping of the Bi2Cr0.5Co0.5Ta2O9+Δ samples, synthesized at temperatures from 650 to 1050 °C; Figure S2: X-ray diffraction patterns of Bi2Co1/2Cr1/2Nb2O9+Δ sample, synthesized at temperatures from 650 to 1050 °C (15 h); Figure S3: Microphotograph and EDS analysis of the Bi2Co1/2Cr1/2Nb2O9+Δ sample calcined at 1050 °C; Table S1: Ratio between pyrochlore and BiNbO4 phases in Bi2Co1/2Cr1/2Nb2O9+Δ samples, sequentially calcined for 10 and 15 h at each temperature step.

Author Contributions: Conceptualization, N.A.Z.; Funding acquisition, V.V.K.; Investigation, N.A.Z. and K.A.B.; Resources, M.G.K., R.I.K. and B.A.M.; Validation, N.A.Z. and V.V.K.; Visualization, M.G.K., N.A.Z. and B.A.M.; Writing—original draft, N.A.Z. and V.V.K. All authors have read and agreed to the published version of the manuscript.

Funding: The reported study was funded by Russian Science Foundation (project No. 17-79-30071).

Data Availability Statement: Not applicable.

Acknowledgments: The authors thank the X-ray Diffraction Center, SPSU, for providing instrumental and computational resources.

Conflicts of Interest: The authors declare no conflict of interest.

References

1. Valant, M.; Babu, G.S.; Vrcon, M.; Kolodiazhnyi, T.; Axelsson, A.-K. Pyrochlore Range from Bi_2O_3-Fe_2O_3-TeO_3 System for LTCC and Photocatalysis and the Crystal Structure of New $Bi_3(Fe_{0.56}Te_{0.44})_3O_{11}$. *J. Am. Ceram. Soc.* **2011**, *95*, 644–650. [CrossRef]
2. Murugesan, S.; Huda, M.N.; Yan, Y.; Al-Jassim, M.M.; Subramanian, V. Band-Engineered Bismuth Titanate Pyrochlores for Visible Light Photocatalysis. *J. Phys. Chem. C* **2010**, *114*, 10598–10605. [CrossRef]
3. Khaw, C.C.; Tan, K.B.; Lee, C.K. High temperature dielectric properties of cubic bismuth zinc tantalate. *Ceram. Intern.* **2009**, *35*, 1473–1480. [CrossRef]
4. Giampaoli, G.; Siritanon, T.; Day, B.; Li, J.; Subramanian, M.A. Temperature in-dependent low loss dielectrics based on quaternary pyrochlore oxides. *Prog. Solid State Chem.* **2018**, *50*, 16–23. [CrossRef]
5. Subramanian, M.A.; Aravamudan, G.; Subba Rao, G.V. Oxide pyrochlores—A review. *Prog. Solid State Chem.* **1982**, *15*, 55–143. [CrossRef]
6. McCauley, R.A. Structural Characteristics of Pyrochlore Formation. *J. Appl. Phys.* **1980**, *51*, 290–294. [CrossRef]
7. Zhuk, N.A.; Sekushin, N.A.; Semenov, V.G.; Fedorova, A.V.; Selyutin, A.A.; Krzhizhanovskaya, M.G.; Lutoev, V.P.; Makeev, B.A.; Kharton, V.V.; Sivkov, D.N.; et al. Dielectric properties, Mössbauer study, ESR spectra of $Bi_2FeTa_2O_{9.5}$ with pyrochlore structure. *J. Alloys Compd.* **2022**, *903*, 163928. [CrossRef]
8. Zhuk, N.A.; Krzhizhanovskaya, M.G.; Koroleva, A.V.; Nekipelov, S.V.; Kharton, V.V.; Sekushin, N.A. Thermal Expansion, XPS Spectra, and Structural and Electrical Properties of a New $Bi_2NiTa_2O_9$ Pyrochlore. *Inorgan. Chem.* **2021**, *60*, 4924–4934. [CrossRef]
9. Jusoh, F.A.; Tan, K.B.; Zainal, Z.; Chen, S.K.; Khaw, C.C.; Lee, O.J.; Balachandran, R.; Ananda Murthy, H.C. Novel pyrochlore-structured bismuth iron antimonates: Structural, impedance and electrochemical studies. *Results Phys.* **2021**, *27*, 104542. [CrossRef]
10. Lufaso, M.W.; Vanderah, T.A.; Pazos, I.M.; Levin, I.; Roth, R.S.; Nino, J.C.; Provenzano, V.; Schenck, P.K. Phase formation, crystal chemistry, and properties in the system Bi_2O_3–Fe_2O_3–Nb_2O_5. *J. Sol. St. Chem.* **2006**, *179*, 3900–3910. [CrossRef]
11. Egorysheva, A.V.; Ellert, O.G.; Maksimov, Y.V.; Volodin, V.D.; Efimov, N.N.; Novotortsev, V.M. Subsolidus phase equilibria and magnetic characterization of the pyrochlore in the Bi_2O_3–Fe_2O_3–Sb_2O_x system. *J. Alloys Compd.* **2013**, *579*, 311–314. [CrossRef]
12. Vanderah, T.A.; Lufaso, M.W.; Adler, A.U.; Levin, I.; Nino, J.C.; Provenzano, V.; Schenck, P.K. Subsolidus phase equilibria and properties in the system Bi_2O_3:Mn_2O_3±x:Nb_2O_5. *J. Sol. St. Chem.* **2006**, *179*, 3467–3477. [CrossRef]
13. Zhuk, N.A.; Krzhizhanovskaya, M.G.; Koroleva, A.V.; Nekipelov, S.V.; Sivkov, D.V.; Sivkov, V.N.; Lebedev, A.M.; Chumakov, R.G.; Makeev, B.A.; Kharton, V.V.; et al. Spectroscopic characterization of cobalt doped bismuth tantalate pyrochlore. *Sol. St. Sci.* **2022**, *125*, 106820. [CrossRef]
14. Greedan, J.E. Frustrated rare earth magnetism: Spin glasses, spin liquids and spin ices in pyrochlore oxides. *J. Alloys Comp.* **2006**, *408–412*, 444–455. [CrossRef]
15. Teng, Z.; Zhu, L.; Tan, Y.; Zeng, S.; Xia, Y.; Wang, Y.; Zhang, H. Synthesis and structures of high-entropy pyrochlore oxides. *J. Eur. Ceram. Soc.* **2020**, *40*, 1639–1643. [CrossRef]
16. Laurita, G.; Hickox-Young, D.; Husremovic, S.; Li, J.; Sleight, A.W.; Macaluso, R.; Rondinelli, J.M.; Subramanian, M.A. Covalency-driven Structural Evolution in the Polar Pyrochlore Series $Cd_2Nb_2O_{7-x}S_x$. *Chem. Mater.* **2019**, *31*, 7626–7637. [CrossRef]
17. Kamba, S.; Porokhonskyy, V.; Pashkin, A.; Bovtun, V.; Petzelt, J.; Nino, J.C.; Trolier-McKinstry, S.; Lanagan, M.T.; Randall, C.A. Anomalous broad dielectric relaxation in $Bi_{1.5}Zn_{1.0}Nb_{1.5}O_7$ pyrochlore. *Phys. Rev. B* **2002**, *66*, 054106. [CrossRef]
18. Valant, M. Dielectric Relaxations in Bi_2O_3-Nb_2O_5-NiO Cubic Pyrochlores. *J. Am. Ceram. Soc.* **2009**, *92*, 955–958. [CrossRef]

19. Ismunandar; Kamiyama, T.; Oikawa, K.; Hoshikawa, A.; Kennedy, B.J.; Kubota, Y.; Kato, K. Static bismuth disorder in $Bi_{2-x}(CrTa)O_{7-y}$. *Mater. Res. Bull.* **2004**, *39*, 553–560. [CrossRef]
20. Zhuk, N.A.; Krzhizhanovskaya, M.G.; Koroleva, A.V.; Reveguk, A.A.; Sivkov, D.V.; Nekipelov, S.V. Thermal expansion, crystal structure, XPS and NEXAFS spectra of Fe-doped bismuth tantalate pyrochlore. *Ceram. Intern.* **2022**, *48*, 14849–14855. [CrossRef]
21. Zhuk, N.A.; Sekushin, N.A.; Krzhizhanovskaya, M.G.; Koroleva, A.V.; Reveguk, A.A.; Nekipelov, S.V.; Sivkov, D.V.; Lutoev, V.P.; Makeev, B.A.; Kharton, V.V.; et al. Cr-doped bismuth tantalate pyrochlore: Electrical and thermal properties, crystal structure and ESR, NEXAFS, XPS spectroscopy. *Mater. Res. Bull.* **2023**, *158*, 112067. [CrossRef]
22. Jusoh, F.A.; Tan, K.B.; Zainal, Z.; Chen, S.K.; Khaw, C.C.; Lee, O.J. Investigation of structural and dielectric properties of subsolidus bismuth iron niobate pyrochlores. *J. Asian Ceram. Soc.* **2020**, *8*, 957–969. [CrossRef]
23. Jusoh, F.A.; Tan, K.B.; Zainal, Z.; Chen, S.K.; Khaw, C.C.; Lee, O.J. Novel pyrochlores in the Bi_2O_3-Fe_2O_3-Ta_2O_5 (BFT) ternary system: Synthesis, structural and electrical properties. *J. Mater. Res. Technol.* **2020**, *9*, 11022–11034. [CrossRef]
24. Chon, M.P.; Tan, K.B.; Khaw, C.C.; Zainal, Z.; Taufiq-Yap, Y.H.; Chen, S.K.; Tan, P.Y. Subsolidus phase equilibria and electrical properties of pyrochlores in the Bi_2O_3–CuO–Ta_2O_5 ternary system. *J. Alloys Compd.* **2016**, *675*, 116–127. [CrossRef]
25. Tan, P.Y.; Tan, K.B.; Khaw, C.C.; Zainal, Z.; Chen, S.K.; Chon, M.P. Phase equilibria and dielectric properties of $Bi_{3+(5/2)x}Mg_{2-x}Nb_{3-(3/2)x}O_{14-x}$ cubic pyrochlores. *Ceram. Intern.* **2014**, *40*, 4237–4246. [CrossRef]
26. Tan, P.Y.; Tan, K.B.; Khaw, C.; Zainal, Z.; Chen, S.K.; Chon, M.P. Structural and electrical properties of bismuth magnesium tantalate pyrochlores. *Ceram. Intern.* **2012**, *38*, 5401–5409. [CrossRef]
27. Youn, H.-J.; Sogabe, T.; Randall, C.A.; Shrout, T.R.; Lanagan, M.T. Phase Relations and Dielectric Properties in the Bi_2O_3-ZnO-Ta_2O_5 System. *J. Am. Ceram. Soc.* **2001**, *84*, 2557–2562. [CrossRef]
28. Khaw, C.C.; Tan, K.B.; Lee, C.K.; West, A.R. Phase equilibria and electrical properties of pyrochlore and zirconolite phases in the Bi_2O_3–ZnO–Ta_2O_5 system. *J. Eur. Ceram. Soc.* **2012**, *32*, 671–680. [CrossRef]
29. Zhuk, N.A.; Krzhizhanovskaya, M.G. Thermal expansion of bismuth magnesium tantalate and niobate pyrochlores. *Ceram. Int.* **2021**, *47*, 30099–30105. [CrossRef]
30. Zhuk, N.A.; Krzhizhanovskaya, M.G.; Sekushin, N.A.; Kharton, V.V.; Makeev, B.A.; Belyy, V.A.; Korolev, R.I. Dielectric performance of pyrochlore-type $Bi_2MgNb_{2-x}Ta_xO_9$ ceramics: The effects of tantalum doping. *Ceram. Intern.* **2021**, *47*, 19424–19433. [CrossRef]
31. Zhuk, N.A.; Krzhizhanovskaya, M.G.; Sekushin, N.A.; Kharton, V.V.; Koroleva, A.V.; Nekipelov, S.V.; Sivkov, D.V.; Sivkov, V.N.; Makeev, B.A.; Lebedev, A.M.; et al. Novel Ni-Doped Bismuth–Magnesium Tantalate Pyrochlores: Structural and Electrical Properties, Thermal Expansion, X-ray Photoelectron Spectroscopy, and Near-Edge X-ray Absorption Fine Structure Spectra. *ACS Omega* **2021**, *6*, 23262–23273. [CrossRef]
32. Zhuk, N.A.; Makeev, B.A.; Korolev, R.I.; Sivkov, D.N.; Shpynova, A.D. A study of phase evolution of Fe-doped bismuth tantalate pyrochlore. *Ceram. Intern.* **2022**, *48*, 31965–31969. [CrossRef]
33. Nino, J.C.; Lanagan, M.T.; Randall, C.A. Phase formation and reactions in the Bi_2O_3–ZnO–Nb_2O_5–Ag pyrochlore system. *J. Mater. Res.* **2001**, *16*, 1460–1464. [CrossRef]
34. Rylchenko, E.P.; Makeev, B.A.; Sivkov, D.V.; Korolev, R.I.; Zhuk, N.A. Features of phase formation of pyrochlore-type $Bi_2Cr_{1/6}Mn_{1/6}Fe_{1/6}Co_{1/6}Ni_{1/6}Cu_{1/6}Ta_2O_{9+\Delta}$. *Lett. Mater.* **2022**, *12*, 486–492. [CrossRef]
35. Zhuk, N.A.; Makeev, B.A.; Krzhizhanovskaya, M.G.; Korolev, R.I. Effect of magnesium and zinc on phase formation of pyrochlore-type $Bi_2Mg(Zn)_{1-x}M_xTa_2O_{9.5-\Delta}$ (M-Cr, Fe) ceramics. *Ceram. Intern.* **2023**, *49*, 5496–5509. [CrossRef]
36. Zhuk, N.A.; Kovalenko, S.Y.; Korolev, R.I.; Makeev, B.A.; Krzhizhanovskaya, M.G.; Sivkov, D.V.; Nekipelov, S.V.; Sivkov, V.N.; Yermolina, M.V. Features of Phase Formation of Pyrochlore-type Ceramics $Bi_2Mg(Zn)_{1-x}Ni_xTa_2O_9$. *ACS Omega* **2023**, *8*, 11351–11363. [CrossRef]
37. Akselrud, L.G.; Grin, Y.N.; Zavalij, P.Y. CSD-universal program package for single crystal or powder structure data treatment. In Proceedings of the 12th European Crystallographic Meeting, Moscow, Russia, 20–29 August 1989; p. 155.
38. Zhuk, N.A.; Krzhizhanovskaya, M.G.; Sekushin, N.A.; Sivkov, D.V.; Abdurakhmanov, I.E. Crystal structure, dielectric and thermal properties of cobalt doped bismuth tantalate pyrochlore. *J. Mater. Res. Technol.* **2023**, *22*, 1791–1799. [CrossRef]
39. Da Cruz, J.A.; Volnistem, E.A.; Ferreira, R.F.; Freitas, D.B.; Sales, A.J.M.; Costa, L.C.; Graça, M.P.F. Structural characterization of Brazilian niobium pentoxide and treatment to obtain the single phase (H-Nb_2O_5). *Therm. Sci. Eng. Progr.* **2021**, *25*, 101015. [CrossRef]
40. Zahid, A.H.; Han, Q. A review on the preparation, microstructure, and photocatalytic performance of Bi_2O_3 in polymorphs. *Nanoscale* **2021**, *13*, 17687–17724. [CrossRef]
41. Gopalakrishnan, J.; Ramanan, A.; Rao, C.N.R.; Jefferson, D.A.; Smith, D.J. A homologous series of recurrent intergrowth structures of the type $Bi_4A_{m+n-2}B_{m+n}O_{3(m+n)+6}$ formed by oxides of the aurivillius family. *Sol. St. Chem.* **1984**, *55*, 101–105. [CrossRef]
42. Grins, J.; Esmaeilzadeh, S.; Hull, S. Structure and Ionic Conductivity of $Bi_6Cr_2O_{15}$, a New Structure Type Containing $(Bi_{12}O_{14})_{8n+n}$ Columns and CrO_4^{2-} Tetrahedra. *J. Sol. St. Chem.* **2002**, *163*, 144–150. [CrossRef]
43. Liu, Y.H.; Li, J.B.; Lianga, J.K.; Luo, J.; Ji, L.N.; Zhang, J.Y.; Rao, G.H. Phase diagram of the Bi_2O_3–Cr_2O_3 system. *Mater. Chem. Phys.* **2008**, *112*, 239–243. [CrossRef]
44. Struzik, M.; Liu, X.; Abrahams, I.; Krok, F.; Malys, M.; Dygas, J.R. Defect structure and electrical conductivity in the pseudo-binary system Bi_3TaO_7–Bi_3NbO_7. *Sol. St. Ion.* **2012**, *218*, 25–30. [CrossRef]

45. Castro, A.; Aguado, E.; Rojo, J.M.; Herrero, P.; Enjalbert, R.; Galy, J. The New Oxygen-Deficient Fluorite Bi_3NbO_7: Synthesis, Electrical Behavior and Structural Approach. *Mater. Res. Bull.* **1998**, *33*, 31–41. [CrossRef]
46. Roth, R.S.; Waring, J.L. Synthesis and stability of bismutotantalite, stibiotantalite and chemically similar ABO_4 compounds. *Am. Mineral.* **1963**, *48*, 1348–1356.
47. Zhuk, N.A.; Krzhizhanovskaya, M.G.; Belyy, V.A.; Makeev, B.A. High-Temperature Crystal Chemistry of α-, β-, and γ-$BiNbO_4$ Polymorphs. *Inorg. Chem.* **2019**, *58*, 1518–1526. [CrossRef]
48. Guragain, D.; Zequine, C.; Gupta, R.K.; Mishra, S.R. Facile Synthesis of Bio-Template Tubular MCo_2O_4 (M = Cr, Mn, Ni) Microstructure and Its Electrochemical Performance in Aqueous Electrolyte. *Processes* **2020**, *8*, 343. [CrossRef]
49. Piir, I.V.; Prikhodko, D.A.; Ignatchenko, S.V.; Schukariov, A.V. Preparation and structural investigations of the mixed bismuth niobates, containing transition metals. *Sol. St. Ion.* **1997**, *101–103*, 1141–1146. [CrossRef]
50. Shannon, R.D. Revised effective ionic radii and systematic studies of interatomic distances in halides and chalcogenides. *Acta Crystallogr. A* **1976**, *32*, 751–767. [CrossRef]
51. Zhuk, N.A.; Krzhizhanovskaya, M.G.; Koroleva, A.V.; Selyutin, A.A.; Sekushin, N.A.; Nekipelov, S.V.; Sivkov, D.V.; Kharton, V.V. Cr and Mg codoped bismuth tantalate pyrochlores: Thermal expansion and stability, crystal structure, electrical and optical properties, NEXAFS and XPS study. *J. Sol. St. Chem.* **2023**, *323*, 124074. [CrossRef]